IJMMM International Journal of Minerals, Metallurgy and Materials 矿物冶金与材料学报（英文版）

A review of linear friction welding of Ni-based superalloys

Xiawei Yang, Tingxi Meng, Qiang Chu, Yu Su, Zhenguo Guo, Rui Xu, Wenlong Fan, Tiejun Ma, and Wenya Li

Cite this article as:
Xiawei Yang, Tingxi Meng, Qiang Chu, Yu Su, Zhenguo Guo, Rui Xu, Wenlong Fan, Tiejun Ma, and Wenya Li, A review of linear friction welding of Ni-based superalloys, *Int. J. Miner. Metall. Mater.*, 31(2024), No. 6, pp. 1382-1391. https://doi.org/10.1007/s12613-023-2782-7

INTERNATIONAL JOURNAL OF
Minerals, Metallurgy and Materials

Volume 31, Number 6, June 2024
Page 1382

Invited Review

https://doi.org/10.1007/s12613-023-2782-7

A review of linear friction welding of Ni-based superalloys

Xiawei Yang[1)], *Tingxi Meng*[1)], *Qiang Chu*[2)], *Yu Su*[1)], *Zhenguo Guo*[1)], *Rui Xu*[1)], *Wenlong Fan*[1)], *Tiejun Ma*[1)], *and Wenya Li*[1),✉]

1) State Key Laboratory of Solidification Processing, Shaanxi Key Laboratory of Friction Welding Technologies, Northwestern Polytechnical University, Xi'an 710072, China

2) Xi'an Aerospace Engine Co. Ltd., Xi'an 710100, China

(Received: 11 August 2023; revised: 21 October 2023; accepted: 8 November 2023)

Abstract: Ni-based superalloys are one of the most important materials employed in high-temperature applications within the aerospace and nuclear energy industries and in gas turbines due to their excellent corrosion, radiation, fatigue resistance, and high-temperature strength. Linear friction welding (LFW) is a new joining technology with near-net-forming characteristics that can be used for the manufacture and repair of a wide range of aerospace components. This paper reviews published works on LFW of Ni-based superalloys with the aim of understanding the characteristics of frictional heat generation and extrusion deformation, microstructures, mechanical properties, flash morphology, residual stresses, creep, and fatigue of Ni-based superalloy weldments produced with LFW to enable future optimum utilization of the LFW process.

Keywords: Ni-based superalloys; linear friction welding; microstructures; mechanical properties; flash morphology

1. Introduction

Ni-based superalloys are widely applied in aerospace and power generation industries, such as gas turbines, modern aero engines, and other high-temperature applications, due to their high-temperature strength, excellent oxidation resistance, and satisfactory corrosion resistance [1–4]. Urgent improvements in engine manufacturing technology for the aviation field are required, and it is particularly important to conduct research on integral blade disk machining and manufacturing technologies. Ni-based superalloys are key materials used in the manufacture of integral blade disks because they meet the requirements of high technical indices and can be used in harsh environments [5–6]. Currently, integral disk manufacturing methods mainly include integral machining (computer numerical control milling and precision casting) and welding (electron beam welding, vacuum diffusion welding, and linear friction welding) [7]. Linear friction welding (LFW) is employed in engine integral disk manufacturing because of its solid phase connection, precision, and environmental protection properties [8–9].

Compared with the disadvantages associated with fusion welding of metals, such as solidification cracking, the segregation of alloy elements, and the existence of pores in the weld zone [10–14], solid-state welding technique does not involve melting or solidification processes; therefore, it avoids the limitations of fusion welding [15–17]. LFW extends the solid-state technology of rotary friction welding to non-axisymmetric components and is suitable for use with different metal combinations [18–21]. Therefore, compared with other joining technologies, LFW is more suitable for manufacturing dual-performance blisks of aeroengines with a high thrust-to-weight ratio. However, the LFW process has certain inherent disadvantages [22]: the method is limited by the shape of the part to be welded, the part to be welded must be able to undergo plastic deformation, and the flash produced during the welding process must be eliminated after welding is completed. Nevertheless, several materials have been successfully joined by LFW, such as steels [23–28], superalloys [29–36], titanium alloys [37–46], and aluminum alloys [47–50].

Li *et al.* [24] investigated the influence of friction time on the flash shape and axial shortening during 45 steel LFW under appropriate welding conditions, and a sound weld with fine microstructures was formed at a friction time of not less than 3 s. Through the reciprocating movement and expulsion of the plasticized material, periodic ridges were formed on the flash edge; those in the direction of friction had a corrugated band structure, and those in the vertical direction had the structure of a small curled vortex. To weld aluminum alloys, Mogami *et al.* [49] developed a high-frequency LFW with an operating frequency of 250 Hz, which is larger than that traditionally used, and studied the relationship between the mechanical properties and the microstructure of the LFW joints of 6063 and 5052 aluminum alloys under different strengthening mechanisms. The change in the flash shape

✉ Corresponding author: Wenya Li Email: liwy@nwpu.edu.cn

with increasing time showed that high-temperature stress resistance and thermal conductivity of the material greatly affected the flow of the material in the joint. LFW has also created a new impetus for the use of nickel-based superalloys [51].

LFW is a process that involves the reciprocal motion between a stationary component and a moving workpiece under a force [31,51–53]. Fig. 1 shows the LFW process [24]. Fig. 1(a) shows the schematic of LFW process. As shown in Fig. 1(b)–(e), the LFW process includes four stages: initial, transition, equilibrium, and deceleration stages. In the initial stage (Fig. 1(b)), the two workpieces move linearly under pressure, and the interface generates heat due to solid friction. In the transition phase (Fig. 1(c)), the metal is continuously extruded from the interface between the two workpieces. At the equilibrium stage (Fig. 1(d)), axial shortening begins to occur, and the material in the heat-affected zone yields due to the friction pressure applied to it. A high temperature occurs at this stage, and a flash forms with a shape that is directly related to the material properties. However, when forging pressure is applied in the deceleration stage (Fig. 1(e)), the samples are brought to a rapid standstill. The final stage strengthens the weld and is a very important stage in the friction welding industry.

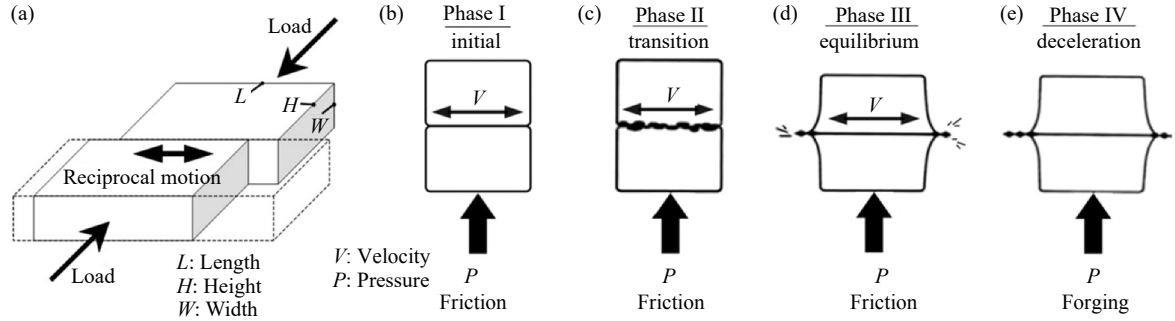

Fig. 1. LFW process [24]: (a) schematic of LFW process; (b) initial stage; (c) transition stage; (d) equilibrium stage; (e) deceleration stage. Reprinted from *Mater. Lett.*, 62, W.Y. Li, T.J. Ma, Q.Z. Xu, *et al.*, Effect of friction time on flash shape and axial shortening of linear friction welded 45 steel, 293-296, Copyright 2008, with permission from Elsevier.

The LFW process provides many advantages for the manufacture of integral blisks [54–56]. For example, compared to traditionally manufactured bladed disk assemblies, which rely on mechanical fasteners and dovetail joints to connect the blade to the disk (as shown in Fig. 2(a)), the LFW method can significantly reduce the weight of components [57–59], as shown in Fig. 2(b), and the lack of a mechanical interface between the blades and disk eliminates the common source of fatigue crack initiation. Furthermore, a linear friction welded (LFWed) blisk improves the gas flow performance [40,56,60–64].

With the development of computer technology, numerical simulations of LFWed Ni-based superalloys have progressed in recent years. Studies of physical models of the LFW process and superalloys have mainly focused on physical simulations of the deformation behavior of the friction and extrusion processes [51,65–69]. The two-dimensional (2D) model provides sufficient information about LFW theoretical problems, including shape characteristics (such as shortening and flash shape) and physical field information (such as that pertaining to the temperature field, stress field, and strain field); as such, it plays an effective role in understanding the basic laws of LFW [51–52,56,70–77]. However, despite these advantages, 2D numerical simulations can only reflect joint deformation behavior from the 2D plane. Therefore, three-dimensional (3D) models are increasingly used by researchers to conduct comprehensive studies of the LFW process [63,68,78–88]. In this respect, Geng *et al.* [68] established a 3D LFW model with 30000 tetrahedral elements and a mesh density that decreased with distance from the contact interface, which saved calculation costs. The results from a 3D LFW simulation based on the strain compensated Arrhenius model showed good agreements with LFW experimental results. As such, this model was considered to be more suitable for use in GH4169 LFW simulations than the other two models (modified F-B and J-C models).

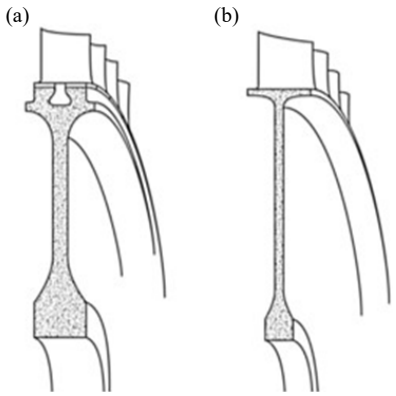

Fig. 2. (a) A conventional bladed disk assembly and (b) a linear friction welded blisk [56]. Reprinted from *Acta Mater.*, 59, R. Turner, J.C. Gebelin, R.M. Ward, and R.C. Reed, Linear friction welding of Ti–6Al–4V: modeling and validation, 3792-3803, Copyright 2011, with permission from Elsevier.

This paper reviews published works on LFWed Ni-based superalloys to understand the characteristics of frictional heat generation and extrusion deformation, the simulation of physical fields, microstructures, mechanical properties, flash morphology, residual stresses, creep, and fatigue associated with Ni-based superalloy weldments. The findings in the published work contribute extensively to understanding the

metallurgical and thermomechanical coupling behavior of dissimilar nickel-based superalloy joints made by the LFW process.

This paper proceeds as follows: simulations and analyses of multiphysical fields during the LFW of Ni-based superalloys are reviewed, studies based on microstructures and the mechanical properties of LFW of Ni-based superalloys are then analyzed, and the flash morphology of LFW of Ni-based superalloys is subsequently investigated. Then the residual stress, creep, and fatigue of the joints of Ni-based superalloys produced using LFW are discussed. In the final section, the future research focus is proposed.

2. Physical simulation of LFW process with Ni-based superalloys

The LFW process is associated with frictional heat generation and extrusion deformation. Yang *et al.* [65] used finite element method (FEM) models and experimental methods to investigate the temperature distribution in the friction interface of GH4169 superalloy. As shown in Fig. 3(a), heat at the friction interface of the specimen was generated in a noncontinuous way; the grinding marks consisted of many randomly distributed pits, and the main grinding types were abrasive wear and adhesive wear. Yang *et al.* [66] conducted a physical simulation study of the interfacial microstructure evolution and the hot compression bonding behavior of GH4169 superalloy joints produced using LFW; as shown in Fig. 3(b), the novel hot isothermal compression bonding tests were performed on a Gleeble-3500 thermal simulator in the temperature range of 970 to 1150°C at a strain rate range of 0.01 to 10 s^{-1}. The macroscopic morphology and the interfacial microstructure evolution of the hot compression GH4169 bonded joints were investigated using an optical microscope (OM) and scanning electron microscope (SEM). Defects in the joint interfaces were also observed by SEM, and the interfacial oxidation of the compression-bonded joints was discussed. Furthermore, Yang *et al.* [67,89] and Geng *et al.* [68] conducted a thermophysical simulation study of the hot deformation behavior and constitutive model of the LFW process with GH4169 superalloy. As shown in Fig. 3(c), the constitutive Arrhenius-type equation model characterized the deformation behavior of the GH4169 superalloy during the LFW compression process. True stress–true strain curves were found to be sensitive to the temperature and strain rate: at the same strain rate, the flow stress increased with a decrease in the temperature; at the same temperature, the flow stress increased with an increase in the strain rate. The constitutive equation parameters of GH4169 under different strains (0.1, 0.2, 0.3, 0.4, 0.5, 0.6, and 0.7) were calculated. The average relative error between the predicted data and the experimental data was approximately 4.6%, and the maximum relative error was less than 17.2%, which indicated that the experimental curves were in good agreement with the calculated curves.

3. Numerical simulation of LFW process with Ni-based superalloys

In practice, many aspects of the LFW process are difficult to measure by experiment, especially phenomena such as the temperature and deformation history relating to the welding interface. In the LFW process, the welding heat sources are concentrated in local areas of the workpiece rather than throughout the entire weldment, which results in extremely uneven heating and cooling of the workpiece. However, the welding heat source and the workpiece are both in relative motion; therefore, the area of the weldment that is heated constantly changes, the metal in the high-temperature zone of welding is always in a strong state of motion, and the temperature at a certain point on the weldment also changes over time. Nevertheless, welding heat sources are usually highly concentrated, and the heating area is small, resulting in extremely fast heating of the workpiece, which causes rapid local heating. Due to the localization of heating and the movement of heat sources, the cooling speed of the workpiece is also very high. The heat transfer process inside the joint is dominated by metal heat conduction, while outside the joint, it is dominated by convective heat transfer. In summary, the welding heat transfer problem is complex due to the LFW thermal processes, and understanding these processes is difficult due to the rapid nature of the process and the fact that the interface of the workpieces cannot be observed during welding. Computational modeling provides a practical method for studying the history of the welding process, allowing an in-depth understanding of the rapid development process [55–56,58,70,90], and physical simulations have been used to study the friction behavior and extrusion deformation characteristics of LFW of Ni-based superalloys [65–67,89]. Numerical models of the LFW process with Ni-based superalloys have also been used to obtain data on various welding responses of those alloys, such as the temperature fields, stress fields, and flash morphology. In this respect, the main advantage of finite element analysis is that it can predict many outputs that are difficult to obtain experimentally.

To study the Mises stress and equivalent plastic strain fields at different welding times, Yang *et al.* [51] conducted friction-wear tests and established a 2D thermomechanical coupling model based on the shear and extrusion deformations characteristics of the LFW process. The authors recorded the actual LFW process of GH4169 and observed the temperature field of the joint surface with a high-speed camera and infrared thermal imager, and finally verified the simulation results through the axial shortening and macroscopic morphology of the LFW joint , where the actual specimen was a block measuring 40 mm (height, H) × 10 mm (length, L) × 18 mm (width, W). In the LFW process, frictional shear stress played a dominant role at a welding time of 0–0.75 s. At a welding time of 0.75–1.65 s, the friction shear stress decreased, and the extrusion pressure increased. Extrusion pressure then played a leading role at a welding time of 1.65–

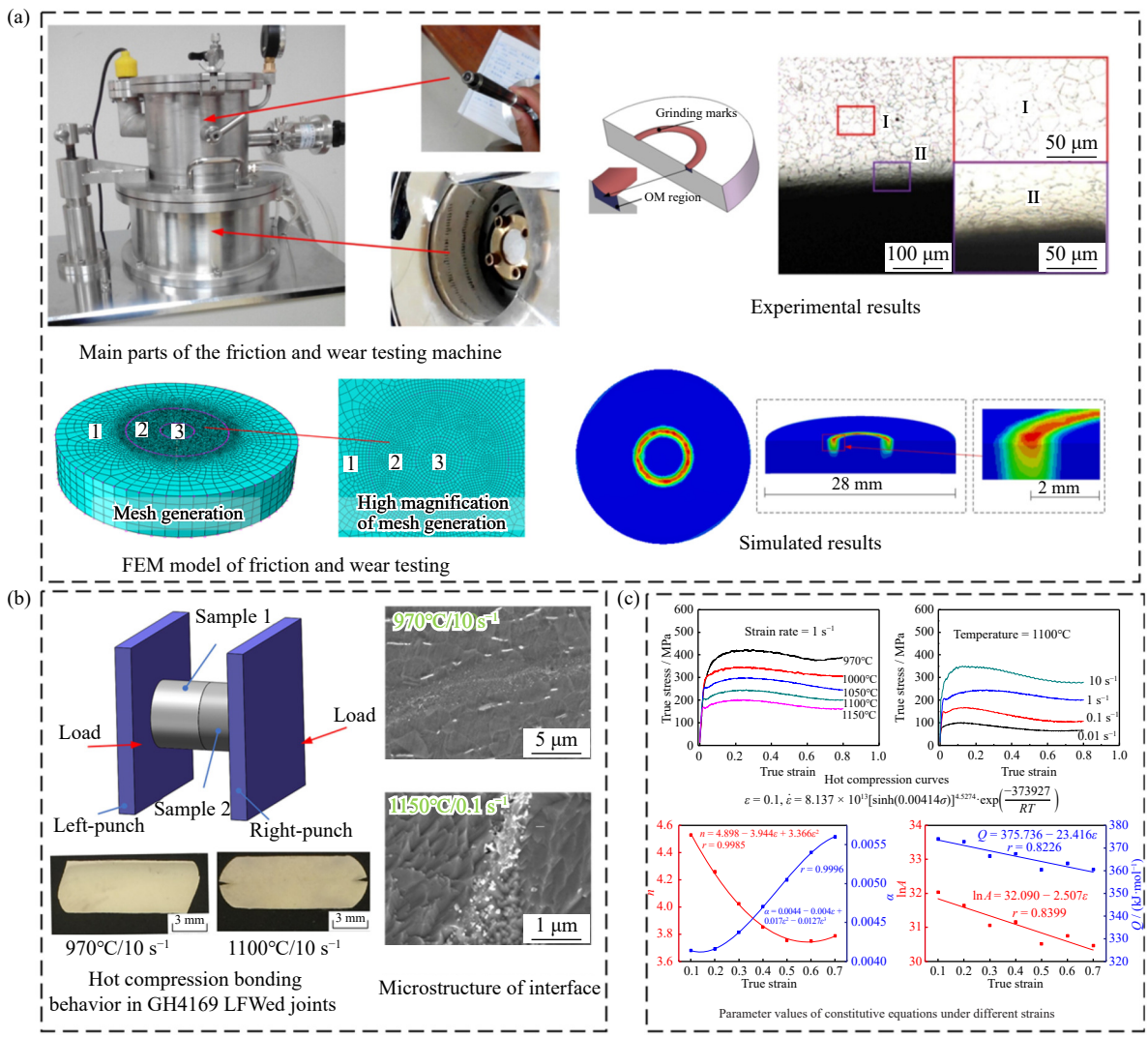

Fig. 3. Physical simulation of LFW process with Ni-based superalloys: (a) temperature and microstructure evolution in friction interface of GH4169 [65]; (b) interfacial microstructure evolution for hot bonding behavior in LFWed joint of GH4169 [66]; (c) constitutive modeling of GH4169 superalloy during LFW process (ε—strain; $\dot{\varepsilon}$—strain rate (s^{-1}); σ—flow stress (MPa); R—gas constant (8.3154 $J \cdot mol^{-1} \cdot K^{-1}$); T—absolute temperature (K); n, α, and A—material constants; Q—deformation activation energy (kJ/mol); r—correlation coefficient) [67]. (a) Reprinted from *Mater. Des.*, 84, X.W. Yang, W.Y. Li, J. Li, *et al.*, FEM analysis of temperature distribution and experimental study of microstructure evolution in friction interface of GH4169 superalloy, 133-143, Copyright 2015, with permission from Elsevier. (b) Reprinted from *Mater. Des.*, 104, X.W. Yang, W.Y. Li, Y. Feng, *et al.*, Physical simulation of interfacial microstructure evolution for hot compression bonding behavior in linear friction welded joints of GH4169 superalloy, 436-452, Copyright 2016, with permission from Elsevier. (c) Reprinted from *J. Alloys Compd.*, 656, X.W. Yang, W.Y. Li, J. Ma, *et al.*, Thermophysical simulation of the compression testing for constitutive modeling of GH4169 superalloy during linear friction welding, 395-407, Copyright 2016, with permission from Elsevier.

1.75 s. The quasi-steady state of the welding process appeared after the welding time exceeded 1.75 s. Geng *et al.* [87,91–92] established a 3D coupled thermomechanical model to simulate the LFW of Ni-based superalloys. The authors used the plastic/plastic friction pair model to consider the full frictional contact interaction between two deformable workpieces to study the temperature gradient, the flow property, and the thermoelastic effects in the LFW process [91–92]. Here, the actual specimen was a block of 33 mm (H), 14 mm (L), and 10 mm (W). Furthermore, the sliding model and sliding-sticking model were respectively used in the FEM model [87] to characterize the friction condition and study morphology of the plastic deformation zone.

To establish optimal welding conditions for the sound LFWed joint integrity of IN718/FGH96 dissimilar superalloys, Geng *et al.* [93] studied the effects of different process parameters on macroscopic and microscopic formation and the evolution and properties of the microstructure. Increasing the oscillation frequency or reducing the applied pressure promoted grain refinement and continuous dynamic recrystallization, although discontinuous dynamic recrystallization remained dominant. The dissolution enhancement of the strengthening phase (δ phase on the IN718 side and γ′ phase on the FGH96 side) was observed from the thermomechanically affected zone to the interface. The main mechanism for enhancing interface bonding was solid solution strengthen-

ing, which was promoted by the mutual deformation of materials on both sides. Furthermore, based on the Johnson–Mehl–Avrami–Kolmogorov recrystallization model, Javidikia *et al.* [94] studied the evolution of the average grain size as a function of the most influential process parameters, and the experimental results were verified.

4. Microstructure and mechanical properties of LFW of Ni-based superalloys

Ma *et al.* [36] conducted LFW experiments with a single-crystal nickel-based superalloy to produce sound welds. In their study, the specimens were cut to the following dimensions: 50 mm (*H*), 19.2 mm (*L*), and 6.25 mm (*W*); the overall cross-sectional microstructure of the joint along the oscillation direction is shown in Fig. 4(a). The weld zone (WZ) was clearly identified, and there were no defects in the weld. In the WZ, the microstructure contained recrystallized polycrystals instead of a single crystal (Fig. 4(b) and (c)). Both elongated and globular γ′ phases existed in the thermomechanically affected zone (TMAZ), and the amount of γ′ was much less than that in the parent material, as shown in Fig. 4(d). The occurrence of γ′ in the middle of the TMAZ (Fig. 4(e)) was lower than at the edges (Fig. 4(d)). It can be seen from Fig. 4(e) that the γ′ phase in the dendritic regions was less than that in the interdendritic regions. As shown in Fig. 4(f), the significant difference in the amount of γ' precipitation within the TMAZ located away from the interface indicated that the temperature field in TMAZ was not uniform. In addition, Ma *et al.* [34] found that fine recrystallized grains in the WZ of the GH4169 LFW joint could be obtained under certain conditions, and the grains in the TMAZ presented no obvious deformation. Moreover, due to the high interface temperature during the welding process, the segregation of certain impurity elements along the grain boundaries and the reversion of γ″ and γ′ resulted in the decline of the mechanical properties of the joint. In addition, a weak layer of oxide and carbide residues was formed at the end of the joint, which was detrimental to the integrity of the joint. Ma *et al.* [31] discovered fine microstructures in the WZ and TMAZ of GH3044 LFW joints and limited oxide at the weld edges under certain welding conditions. The flow line feature was present in the WZ and TMAZ due to carbide rearrangement, and the microhardness and tensile strength of the joints were higher than those of the base metal (BM). The weld microstructure during the LFW process underwent discontinuous dynamic recrystallization, accompanied by limited continuous dynamic and static recrystallization, resulting in a significant increase in the proportion of low-angle grain boundaries (LAGBs) and a dramatic decrease in the proportion of Σ3 twin boundaries in WZ and TMAZ. Karadge *et al.* [30] investigated the effects of crystal orientation on weldability and microstructural evolution during LFW of single-crystal nickel-based superalloy to polycrystalline nickel-based superalloy. In their paper, deformation and the microstructure development were observed by electron microscope. The friction coefficient varied with crystal orientation and was related to metallurgical adhesion. These changes were explained by considering the mechanism of single-crystal deformation. During the LFW process, the orientation of the single crystal

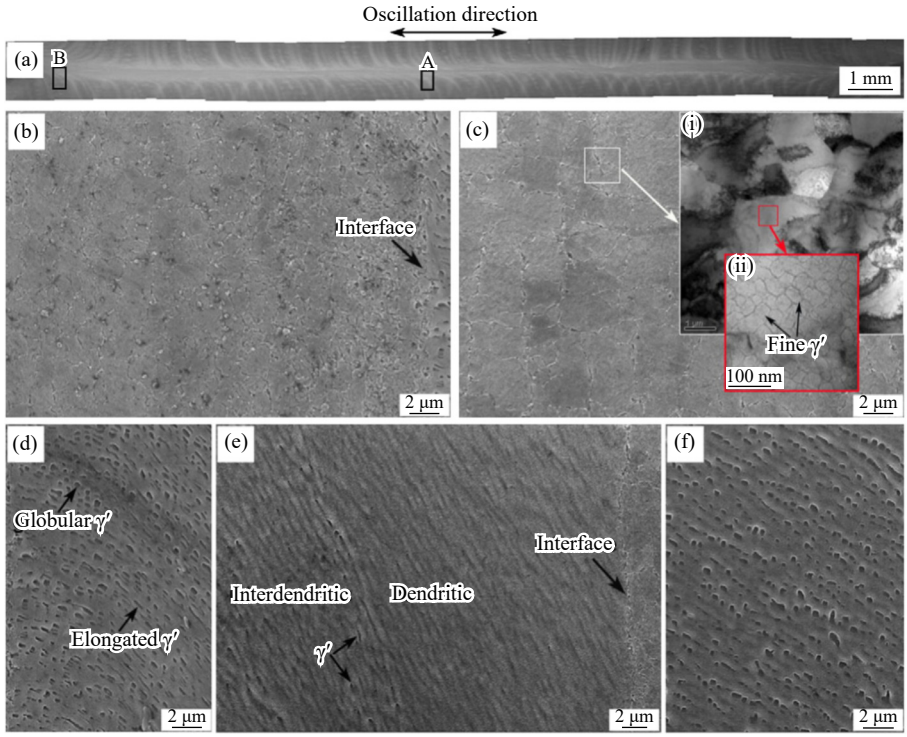

Fig. 4. (a) Overall view of the weld with OM; (b) high magnification of the WZ in zone B;(c) high magnification of the WZ in zone A; (d) high magnification of the TMAZ in zone B; (e, f) high magnification of the TMAZ in zone A (f is further away from the interface) [36]. Reprinted from *Mater. Des.*, 85, T.J. Ma, M. Yan, X.W. Yang, *et al.*, Microstructure evolution in a single crystal nickel-based superalloy joint by linear friction welding, 613-617, Copyright 2015, with permission from Elsevier.

relative to the pressure axis was important due to the orientation change of the primary slip system in the fcc-based single crystal lattice.

Masoumi *et al.* [95] and Ye *et al.* [35] respectively studied the microstructure evolution and mechanical testing of the superalloy joints welded with LFW before and after heat treatment. Tabaie *et al.* [96–97] used LFW to weld the elective laser melted (SLM) Inconel718 (IN718) superalloy and the forged AD730™ nickel-based superalloy. The microstructure was evaluated, especially in terms of the grain size and orientation differences, and changes in the different areas of the WZ were studied and correlated with the evolution of microhardness. Geng *et al.* [98] found that refined grains were observed in the weld seam of GH4169 joints welded with LFW due to dynamic recrystallization (DRX). The δ phase gradually dissolved from the BM to the weld interface, where almost no δ phase exists. Discontinuous DRX mainly occurred in the welding zone, accompanied by limited continuous DRX. Furthermore, Geng *et al.* [99] investigated the microstructural evolution and microhardness in LFW of FGH4096 and GH4169 superalloys. Complete DRX was achieved in the friction interface zone, and there were no obvious secondary phases (including δ and carbide phases) on the GH4169 side, and no primary and secondary γ' phases on the FGH4096 side. The TMAZ showed incomplete DRX with significantly lower amounts of LAGBs and partially dissolved secondary phases depending on the distance from the weld line.

Chamanfar *et al.* [100] studied the tensile properties and microhardness of nickel-base superalloy (Waspaloy) linear friction welded (LFWed) joints and compared those with the post-weld heat treatment (PWHTed) state. The results showed that in the weld area consisting of the weld interface and the TMAZ, γ′ dissolution occurred and led to softening. Grain refinement occurred in the entire weld area due to dynamic recrystallization and the increase in axial shortening, and the finer the grains, the higher the yield strength (YS), and the lower the elongation. The applied post-weld heat treatment (PWHT) recovered the dissolved γ′ particles and resulted in significant increases in the YS and ultimate tensile strength (UTS) of the weldment. In addition, the stored energy in the welding zone was relaxed, grain growth occurred in the weld area during PWHT, and there was an improvement in the elongation of linear friction welds after heat treatment.

5. Flash morphology of LFW of Ni-based superalloys

Yonekura *et al.* [88] discussed the importance of the flash path for the quality of LFWed joints; they studied the flash extrusion path through experiments and demonstrated that flash tends to flow toward the nearest edge. Based on such observations, a mathematical model of flash extrusion was established, and a Voronoi diagram based on the flash extrusion prediction method was proposed. Geng *et al.* [99] established a thermomechanical coupling model to predict the temperature, plastic strain, and stress distribution during LFW of FGH4096 and GH4169 superalloys. They compared the cross-sectional morphology and flash shape between the experiment and simulation at different friction pressures, and the results showed that the difference in the average error percentage of the total shortened length of the four joints was less than 8%, indicating a satisfactory match between the predicted and the measured deformation.

6. Residual stresses, creep, and fatigue

Smith *et al.* [101] analyzed the elastic residual stress of IN 718 linear friction welds, where the dimensions of the specimen were 9 mm (*H*), 34 mm (*L*), and 12.5 mm (*W*). The evolution in the residual strains and stresses in the heat-affected zone (HAZ), TMAZ, and DRX of the weld was investigated using the neutron diffraction and contour methods. The results indicated that the magnitude of residual stress originating from the BM increased and reached a peak at the welding interface. In addition, the peak amplitude of the residual stress was lower than the yield stress of IN 718. Furthermore, Masoumi *et al.* [102] conducted high-temperature creep tests on AD730™ Ni-based superalloy as-welded and post-weld heat-treated (PWHTed) joints at two different temperatures: 700°C under 600 and 750 MPa stress levels, and 850°C under 100 and 200 MPa stresses. Here, the dimensions of the specimen were 37 mm (*H*), 26 mm (*L*), and 13 mm (*W*). The creep resistance of the PWHTed joints was higher than that of the welded specimens. The PWHTed joints exhibited better ductility than the BM at 850°C, while they exhibited slightly lower creep life compared to the BM at 700°C. Furthermore, Yang *et al.* [103] used the FEM to investigate the fatigue crack growth behavior of an LFWed superalloy joint and its important influencing factors (the dimensions of the actual block specimen were 55 mm (*H*), 12 mm (*L*), and 18 mm (*W*)). The authors considered the source of joint failures, such as voids, hard inclusions, and residual stress, and established a finite element model of fatigue joints with different geometric and positional features containing initial voids and inclusions. The order of crack initiation and propagation in fatigue joints under different characteristics was studied, and the important factor levels of crack propagation were classified.

Chen *et al.* [104] studied the residual stress of a single crystal nickel superalloy CMSX-4 TIG welding joint. By comparing the residual stress of a single crystal nickel superalloy CMSX-4 TIG welded joint and an IN 718 LFWed joint, the authors found that the residual stress of LFWed joints was lower than that of fusion welded joints. During creep tests, Pasiowiec *et al.* [105] investigated the microstructure evolution of Inconel 625 additively manufactured by laser powder bed fusion (LPBF); In this paper [105], it is evident that a constant negative strain was found after a short incubation time of approximately 20 h during the creep test at 600°C/100 MPa. The creep curve of the specimen tested at

700°C/100 MPa shows that the initial phase of the second creep phase occurred at about 700 h, and the strain was relatively low (at about 0.6%) after the creep test had continued for 2000 h. In the 800°C creep test, fracture occurred after 240 h, and the creep curve shows a dominant tertiary creep stage and a short secondary creep rate occurred at 30–100 h. Wen *et al.* [106] investigated the typical fatigue fracture morphologies of GH4169 electron beam welded (EBWed) joints at various temperatures. All the fatigue cracks were caused by welding defects in relation to the stress concentration, as represented by the red ellipse. In their study [106], the types of welding defects were divided into four categories according to the characteristics and location of defects: surface welding cracks, surface welding inclusions, surface welding pores, and internal welding pores.

7. Recommendations for further research

Although recent progress has been made in understanding Ni-based superalloys LFW, existing knowledge gaps need to be addressed to assist our understanding of the associated processes and to improve the industrial implementation of LFW. We suggest that research should focus on the following areas.

(1) Oxygen elements effects. The LFW process occurs over a short time at a high strain rate. The interface temperature rises quickly, and there is a large temperature gradient. In consideration of the temperature factors during the welding process, the diffusion mode, path, and depth of the oxygen elements affect the microstructure and properties of the joint. In addition, the action of oxygen elements can alter the chemical composition of the joint and its impact on the initiation and propagation behavior of defects in the joint.

(2) Microstructural simulation methods. Computer modeling, numerical or visual simulation, and microstructural simulation can be used to study the evolution process and mechanism of microstructures, as well as the basic characteristics of materials at the micro or mesoscale. Models can be used to study the influence of processing conditions on the evolution of microstructure; this enables the characterization of the effects of processing conditions on various phases, the average grain size, the grain microstructure, and the grain spatial distribution of Ni-based superalloy welds.

(3) Near-net-forming. LFW technology has good application prospects in near-net-forming. By designing special clamps to splice small pieces into large components, it can overcome the disadvantages of fusion welding (performance degradation at welded joints), and this is a suggested future research direction.

(4) LFW of aeroengine blisks. At present, the challenges faced by the LFW of aeroengine blisks are mainly divided into the following aspects: first, it is difficult to control the accuracy, including the joint forming accuracy and axial shortening accuracy at the end of welding. Second, the process of removing excess flash from joints is problematic, and it is essential to ensure that the blades are not damaged during flash removal. Third, the overall heat treatment process for relieving residual stress after welding can severely deform the blades, and implementing local heat treatment is the key to reduce the deformation of the welded parts.

Acknowledgements

This work was financially supported by the National Natural Science Foundation of China (Nos. 52074228, 52305420, and 51875470), the China Postdoctoral Science Foundation (No. 2023M742830), and the Xi'an Beilin District Science and Technology Planning Project, China (No. GX2349).

Conflict of Interest

Wenya Li is an editorial board member for this journal and was not involved in the editorial review or the decision to publish this article. The authors declare no conflict of interest.

References

[1] S.L. Yang, S.F. Yang, W. Liu, *et al*., Microstructure, segregation and precipitate evolution in directionally solidified GH4742 superalloy, *Int. J. Miner. Metall. Mater.*, 30(2023), No. 5, p. 939.

[2] H.H. Tayeband and S.M. Rafiaei, Enhanced microstructural and mechanical properties of Stellite/WC nanocomposite on Inconel 718 deposited through vibration-assisted laser cladding, *Int. J. Miner. Metall. Mater.*, 29(2022), No. 2, p. 327.

[3] M.H. Zhang, B.C. Zhang, Y.J. Wen, *et al*., Research progress on selective laser melting processing for nickel-based superalloy, *Int. J. Miner. Metall. Mater.*, 29(2022), No. 3, p. 369.

[4] E.Y. Liu, Q.S. Ma, X.T. Li, *et al*., Effect of two-step solid solution on microstructure and δ phase precipitation of Inconel 718 alloy, *Int. J. Miner. Metall. Mater*., (2024). DOI: 10.1007/s12613-024-2887-7

[5] J. Kang, R.G. Li, D.Y. Wu, *et al*., On the low cycle fatigue behaviors of Ni-based superalloy at room temperature: Deformation and fracture mechanisms, *Mater. Charact*, 211(2024), art. No. 113920.

[6] Y. Su, X.W. Yang, T.X. Meng, *et al*., Strengthening mechanism and forming control of linear friction welded GH4169 alloy joints, *Chin. J. Aeronaut.*, 37(2024), No. 4, p. 609.

[7] H.Y. Zhang and L.F. Zhang, Development overview of aeroengine integral blisk and its manufacturing technology at home and abroad, *Aeronaut. Manuf. Technol.*, 56(2013), No. 23/24, p. 38.

[8] M. Smith, L. Bichler, J. Gholipour, and P. Wanjara, Mechanical properties and microstructural evolution of in-service Inconel 718 superalloy repaired by linear friction welding, *Int. J. Adv. Manuf. Technol.*, 90(2017), No. 5-8, p. 1931.

[9] H. Wu, M. Sun, and Y. Yang. Research progress in linear friction welding technology, *Welding Technol.*, 43(2014) No. 7, p. 1.

[10] Z.L. Yi, J.G. Shan, Y. Zhao, *et al*, Recent research progress in the mechanism and suppression of fusion welding-induced liquation cracking of nickel based superalloys, *Int. J. Miner. Metall. Mater*, 31(2024), No. 5, p. 1072.

[11] X.S. Li, D. Sukhomlinov, and Z.Q. Que, Microstructure and

thermal properties of dissimilar M300–CuCr1Zr alloys by multi-material laser-based powder bed fusion, *Int. J. Miner. Metall. Mater.*, 31(2024), No. 1, p. 118.

[12] M.M. Chen, R.H. Shi, Z.Z. Liu, *et al*., Phase-field simulation of lack-of-fusion defect and grain growth during laser powder bed fusion of Inconel 718, *Int. J. Miner. Metall. Mater.*, 30(2023), No. 11, p. 2224.

[13] Y. Su, X.W. Yang, D. Wu, *et al*., Controlling deformation and residual stresses in a TIG joint for Invar steel molds, *J. Mater. Res. Technol.*, 27(2023), p. 490.

[14] Y. Su, X.W. Yang, D. Wu, *et al*., Optimizing welding sequence of TIG cross-joint of Invar steel using residual stresses and deformations, *J. Manuf. Process.*, 105(2023), p. 232.

[15] Z.G. Guo, T.J. Ma, X.W. Yang, *et al*., Linear friction welding of Ti60 near-α titanium alloy: Investigating phase transformations and dynamic recrystallization mechanisms, *Mater. Charact.*, 194(2022), art. No. 112424.

[16] Z.G. Guo, T.J. Ma, W.Y. Li, *et al*., Intergrowth bonding mechanism and mechanical property of linear friction welded dissimilar near-alpha to near-beta titanium alloy joint, *Adv. Eng. Mater.*, 23(2021), No. 5, art. No. 2001479.

[17] X.W. Yang, T.X Meng, Y. Su, *et al*., Evolution of microstructure and mechanical properties of cold spray additive manufactured aluminum deposit on copper substrate, *Mater. Sci. Eng. A*, 891(2024), art. No. 146024.

[18] Z.G. Guo, T.J. Ma, X.W. Yang, *et al*., In-situ investigation on dislocation slip concentrated fracture mechanism of linear friction welded dissimilar Ti17(α + β)/Ti17(β) titanium alloy joint, *Mater. Sci. Eng. A*, 872(2023), art. No. 144991.

[19] Z.G. Guo, T.J. Ma, X. Chen, *et al*., Interfacial bonding mechanism of linear friction welded dissimilar Ti_2AlNb–Ti60 joint: Grain intergrowth induced by combined effects of dynamic recrystallization, phase transformation and elemental diffusion, *J. Mater. Res. Technol.*, 24(2023), p. 5660.

[20] Z.G. Guo, T.J. Ma, X.W. Yang, J. Li, W.Y. Li, and A. Vairis, Multi-scale analyses of phase transformation mechanisms and hardness in linear friction welded Ti17(α + β)/Ti17(β) dissimilar titanium alloy joint, *Chin. J. Aeronaut.*, 37(2024), No. 1, p. 312.

[21] X.W. Yang, S.T. Ma, Q. Chu, *et al*., Investigation of microstructure and mechanical properties of GH4169 superalloy joint produced by linear friction welding, *J. Mater. Res. Technol.*, 24(2023), p. 8373.

[22] M. Orłowska, L. Olejnik, D. Campanella, *et al*., Application of linear friction welding for joining ultrafine grained aluminium, *J. Manuf. Process.*, 56(2020), p. 540.

[23] X.W. Yang, W.Y. Li, and T.J. Ma, Finite element analysis of the effect of micro-pore defect on linear friction welding of medium carbon steel, *China Weld.*, 23(2014), No. 1, p. 1.

[24] W.Y. Li, T.J. Ma, S.Q. Yang, *et al*., Effect of friction time on flash shape and axial shortening of linear friction welded 45 steel, *Mater. Lett.*, 62(2008), No. 2, p. 293.

[25] T.J. Ma, Y.G. Li, W.Y. Li, Y. Zhang, D.G. Shi, and A. Vairis, Studies of the interfacial structure of a linear friction welded Fe/Ni joint: First principles calculation and TEM validation, *Mater. Charact.*, 129(2017), p. 60.

[26] Y.M. Li, Y.C. Liu, C.X. Liu, *et al*., Microstructure evolution and mechanical properties of linear friction welded S31042 heat-resistant steel, *J. Mater. Sci. Technol.*, 34(2018), No. 4, p. 653.

[27] Y. Su, W.Y. Li, X.Y. Wang, *et al*., On the process variables and weld quality of a linear friction welded dissimilar joint between S31042 and S34700 austenitic steels, *Adv. Eng. Mater.*, 21(2019), No. 7, art. No. 1801354.

[28] T. J. Ma, W. Y. Li, Q. Z. Xu, *et al*., Microstructure evolution and mechanical properties of linear friction welded 45 steel joint, *Adv. Eng. Mater.*, 9(2007), No. 8, p. 703.

[29] X.W. Yang, T.X. Meng, Y. Su, *et al*., The effect of inclusions and pores on creep crack propagation of linear friction welded joints of GH4169 superalloy, *J. Mater. Res. Technol.*, 29(2024), p. 4636.

[30] M. Karadge, M. Preuss, P.J. Withers, and S. Bray, Importance of crystal orientation in linear friction joining of single crystal to polycrystalline nickel-based superalloys, *Mater. Sci. Eng. A*, 491(2008), No. 1-2, p. 446.

[31] T.J. Ma, L.F. Tang, W.Y. Li, Y. Zhang, Y. Xiao, and A. Vairis, Linear friction welding of a solid-solution strengthened Ni-based superalloy: Microstructure evolution and mechanical properties studies, *J. Manuf. Process.*, 34(2018), p. 442.

[32] P.H. Geng, G.L. Qin, H. Ma, *et al*., Numerical modelling on the plastic flow and interfacial self-cleaning in linear friction welding of superalloys, *J. Mater. Process. Technol.*, 296(2021), art. No. 117198.

[33] A. Chamanfar, M. Jahazi, J. Gholipour, P. Wanjara, and S. Yue, Suppressed liquation and microcracking in linear friction welded WASPALOY, *Mater. Des.*, 36(2012), p. 113.

[34] T.J. Ma, X. Chen, W.Y. Li, X.W. Yang, Y. Zhang, and S.Q. Yang, Microstructure and mechanical property of linear friction welded nickel-based superalloy joint, *Mater. Des.*, 89(2016), p. 85.

[35] R.R. Ye, H.Y. Li, R.G. Ding, *et al*., Microstructure and microhardness of dissimilar weldment of Ni-based superalloys IN718-IN713LC, *Mater. Sci. Eng. A*, 774(2020), art. No. 138894.

[36] T.J. Ma, M. Yan, X.W. Yang, W.Y. Li, and Y.J. Chao, Microstructure evolution in a single crystal nickel-based superalloy joint by linear friction welding, *Mater. Des.*, 85(2015), p. 613.

[37] X.M. Chen, C. Lin Y., M.S. Chen, *et al.*, Microstructural evolution of a nickel-based superalloy during hot deformation, *Mater. Des*., 77(2015), p. 41.

[38] W.Y. Li, T.J. Ma, Y. Zhang, *et al*., Microstructure characterization and mechanical properties of linear friction welded Ti-6Al-4V alloy, *Adv. Eng. Mater.*, 10(2008), No. 1-2, p. 89.

[39] P. Wanjara and M. Jahazi, Linear friction welding of Ti–6Al–4V: Processing, microstructure, and mechanical-property inter-relationships, *Metall. Mater. Trans. A*, 36(2005), No. 8, p. 2149.

[40] M. Karadge, M. Preuss, C. Lovell, P.J. Withers, and S. Bray, Texture development in Ti–6Al–4V linear friction welds, *Mater. Sci. Eng. A*, 459(2007), No. 1-2, p. 182.

[41] C.C. Zhang, T.C. Zhang, Y.J. Ji, and J.H. Huang, Effects of heat treatment on microstructure and microhardness of linear friction welded dissimilar Ti alloys, *Trans. Nonferrous Met. Soc. China*, 23(2013), No. 12, p. 3540.

[42] J. Romero, M.M. Attallah, M. Preuss, M. Karadge, and S.E. Bray, Effect of the forging pressure on the microstructure and residual stress development in Ti–6Al–4V linear friction welds, *Acta Mater.*, 57(2009), No. 18, p. 5582.

[43] E. Dalgaard, P. Wanjara, J. Gholipour, X. Cao, and J.J. Jonas, Linear friction welding of a near-β titanium alloy, *Acta Mater.*, 60(2012), No. 2, p. 770.

[44] W.Y. Li, T.J. Ma, and S.Q. Yang, Microstructure evolution and mechanical properties of linear friction welded Ti–5Al–2Sn–2Zr–4Mo–4Cr (Ti17) titanium alloy joints, *Adv. Eng. Mater.*, 12(2010), No. 1-2, p. 35.

[45] X. Chen, F.Q. Xie, T.J. Ma, W.Y. Li, and X.Q. Wu, Oxidation behavior of three different zones of linear friction welded Ti_2AlNb alloy, *Adv. Eng. Mater.*, 18(2016), No. 11, p. 1944.

[46] H. Peng, Y.X. Wu, T. Zhang, S.Y. Chen, and C. Zhang, Residual stresses in linear friction welding of TC17 titanium alloy

considering phase fraction, *Trans. Nonferrous Met. Soc. China*, 34(2024), No. 1, p. 184.
[47] F. Rotundo, A. Marconi, A. Morri, and A. Ceschini, Dissimilar linear friction welding between a SiC particle reinforced aluminum composite and a monolithic aluminum alloy: Microstructural, tensile and fatigue properties, *Mater. Sci. Eng. A*, 559(2013), p. 852.
[48] A. Lis, H. Mogami, T. Matsuda, *et al*., Hardening and softening effects in aluminium alloys during high-frequency linear friction welding, *J. Mater. Process. Technol.*, 255(2018), p. 547.
[49] H. Mogami, T. Matsuda, T. Sano, R. Yoshida, H. Hori, and A. Hirose, High-frequency linear friction welding of aluminum alloys, *Mater. Des.*, 139(2018), p. 457.
[50] G. Buffa, M. Cammalleri, D. Campanella, and L. Fratini, Shear coefficient determination in linear friction welding of aluminum alloys, *Mater. Des.*, 82(2015), p. 238.
[51] X.W. Yang, W.Y. Li, J.L. Li, *et al*., Finite element modeling of the linear friction welding of GH4169 superalloy, *Mater. Des.*, 87(2015), p. 215.
[52] A. Vairis and M. Frost, Modelling the linear friction welding of titanium blocks, *Mater. Sci. Eng. A*, 292(2000), No. 1, p. 8.
[53] A. Vairis and M. Frost, High frequency linear friction welding of a titanium alloy, *Wear*, 217(1998), No. 1, p. 117.
[54] A. Vairis and M. Frost, On the extrusion stage of linear friction welding of Ti 6Al 4V, *Mater. Sci. Eng. A*, 271(1999), p. 477.
[55] A.R. McAndrew, P.A. Colegrove, C. Bühr, B. C.D. Flipo, and A. Vairis, A literature review of Ti–6Al–4V linear friction welding, *Prog. Mater. Sci.*, 92 (2018), p. 225.
[56] R. Turner, J.C. Gebelin, R.M. Ward, and R.C. Reed, Linear friction welding of Ti–6Al–4V: Modelling and validation, *Acta Mater.*, 59(2011), No. 10, p. 3792.
[57] J.T. Liu, J.L. Li, X.G. Li, *et al*., Fatigue fracture behavior of a Ti17 joint under various heat treatment specifications prepared by linear friction welding, *Mater. Charact.*, 205(2023), art. No. 113318.
[58] R. Turner, R.M. Ward, R. March, and R.C. Reed, The magnitude and origin of residual stress in Ti–6Al–4V linear friction welds: An investigation by validated numerical modeling, *Metall. Mater. Trans. B*, 43(2012), No. 1, p. 186.
[59] X. Zhang, J.J. Zhang, Y.K. Yao, *et al.*, Anomalous enhancing effects of electric pulse treatment on strength and ductility of TC17 linear friction welding joints, *J. Mater. Sci. Technol*, 203(2024), p. 155.
[60] Z.Y. Dang, G.L. Qin, H. Ma, and P.H. Geng, Multi-scale characterizations of microstructure and mechanical properties of Ti6242 alloy linear friction welded joint with post-welded heat treatment, *Trans. Nonferrous Met. Soc. China*, 33(2023), No. 4, p. 1114.
[61] T.J. Ma, W.Y. Li, and S.Y. Yang, Impact toughness and fracture analysis of linear friction welded Ti–6Al–4V alloy joints, *Mater. Des.*, 30(2009), No. 6, p. 2128.
[62] W.Y. Li, H. Wu, T.J. Ma, C.L. Yang, and Z.W. Chen, Influence of parent metal microstructure and post-weld heat treatment on microstructure and mechanical properties of linear friction welded Ti–6Al–4V joint, *Adv. Eng. Mater.*, 14(2012), No. 5, p. 312.
[63] M. Grujicic, G. Arakere, B. Pandurangan, C.F. Yen, and B.A. Cheeseman, Process modeling of Ti–6Al–4V linear friction welding (LFW), *J. Mater. Eng. Perform.*, 21(2012), No. 10, p. 2011.
[64] P. Frankel, M. Preuss, A. Steuwer, P.J. Withers, and S. Bray, Comparison of residual stresses in Ti–6Al–4V and Ti–6Al–2Sn–4Zr–2Mo linear friction welds, *Mater. Sci. Technol.*, 25(2009), No. 5, p. 640.
[65] X.W. Yang, W.Y. Li, J. Li, T.J. Ma, and J. Guo, FEM analysis of temperature distribution and experimental study of microstructure evolution in friction interface of GH4169 superalloy, *Mater. Des.*, 84(2015), p. 133.
[66] X.W. Yang, W.Y. Li, Y. Feng, S.Q. Yu, and B. Xiao, Physical simulation of interfacial microstructure evolution for hot compression bonding behavior in linear friction welded joints of GH4169 superalloy, *Mater. Des.*, 104(2016), p. 436.
[67] X.W. Yang, W.Y. Li, J. Ma, *et al*., Thermo-physical simulation of the compression testing for constitutive modeling of GH4169 superalloy during linear friction welding, *J. Alloys Compd.*, 656(2016), p. 395.
[68] P.H. Geng, G.L. Qin, J. Zhou, and Z.D. Zou, Hot deformation behavior and constitutive model of GH4169 superalloy for linear friction welding process, *J. Manuf. Process.*, 32(2018), p. 469.
[69] G.L. Qin, P.H. Geng, J. Zhou, and Z.D. Zou, Modeling of thermo-mechanical coupling in linear friction welding of Ni-based superalloy, *Mater. Des.*, 172(2019), art. No. 107766.
[70] W.Y. Li, T.J. Ma, and J.L. Li, Numerical simulation of linear friction welding of titanium alloy: Effects of processing parameters, *Mater. Des.*, 31(2010), No. 3, p. 1497.
[71] W.Y. Li, S.X. Shi, F.F. Wang, *et al*., Heat reflux in flash and its effect on joint temperature history during linear friction welding of steel, *Int. J. Therm. Sci.*, 67(2013), p. 192.
[72] X. Song, M. Xie, F. Hofmann, *et al*., Residual stresses in Linear Friction Welding of aluminium alloys, *Mater. Des.*, 50(2013), p. 360.
[73] A.R. McAndrew, P.A. Colegrove, A.C. Addison, B.C.D. Flipo, M.J. Russell, and L.A. Lee, Modelling of the workpiece geometry effects on Ti–6Al–4V linear friction welds, *Mater. Des.*, 87(2015), p. 1087.
[74] A.R. McAndrew, P.A. Colegrove, A.C. Addison, B.C.D. Flipo, and M.J. Russell, Modelling the influence of the process inputs on the removal of surface contaminants from Ti–6Al–4V linear friction welds, *Mater. Des.*, 66(2015), p. 183.
[75] P. Effertz, F. Fuchs, and N. Enzinger, 3D modelling of flash formation in linear friction welded 30CrNiMo8 steel chain, *Metals*, 7(2017), No. 10, art. No. 449.
[76] P. Jedrasiak, H.R. Shercliff, A.R. McAndrew, and P.A. Colegrove, Thermal modelling of linear friction welding, *Mater. Des.*, 156(2018), p. 362.
[77] P.S. Effertz, F. Fuchs, and N. Enzinger, The influence of process parameters in linear friction welded 30CrNiMo8 small cross-section: A modelling approach, *Sci. Technol. Weld. Join.*, 24(2019), No. 2, p. 121.
[78] J.S.Müller, M. Rettenmayr, D. Schneefeld, O. Roder, and W. Fried, FEM simulation of the linear friction welding of titanium alloys, *Comput. Mater. Sci.*, 48(2010), No. 4, p. 749.
[79] L. Fratini, G. Buffa, D. Campanella, and D. La Spisa, Investigations on the linear friction welding process through numerical simulations and experiments, *Mater. Des.*, 40(2012), p. 285.
[80] M. Grujicic, R. Yavari, J.S. Snipes, S. Ramaswami, C.F. Yen, and B.A. Cheeseman, Linear friction welding process model for carpenter custom 465 precipitation-hardened martensitic stainless steel, *J. Mater. Eng. Perform.*, 23(2014), No. 6, p. 2182.
[81] W.Y. Li, F.F. Wang, S.X. Shi, T.J. Ma, J.L. Li, and A. Vairis, 3D finite element analysis of the effect of process parameters on linear friction welding of mild steel, *J. Mater. Eng. Perform.*, 23(2014), No. 11, p. 4010.
[82] M. Grujicic, R. Yavari, J.S. Snipes, and S. Ramaswami, A linear friction welding process model for Carpenter Custom 465 precipitation-hardened martensitic stainless steel: a weld mi-

crostructure-evolution analysis, *Proc. Inst. Mech. Eng. Part B: J. Eng. Manuf.*, 229(2015), p. 1997.

[83] G. Buffa, D. Campanella, S. Pellegrino, and L. Fratini, Weld quality prediction in linear friction welding of AA6082-T6 through an integrated numerical tool, *J. Mater. Process. Technol.*, 231(2016), p. 389.

[84] A.R. McAndrew, P.A. Colegrove, B.C.D. Flipo, and C. Bühr, 3D modelling of Ti–6Al–4V linear friction welds, *Sci. Technol. Weld. Join.*, 22(2017), No. 6, p. 496.

[85] C. Bühr, B. Ahmad, P.A. Colegrove, A.R. McAndrew, H. Guo, and X. Zhang, Prediction of residual stress within linear friction welds using a computationally efficient modelling approach, *Mater. Des.*, 139(2018), p. 222.

[86] D. Baffari, G. Buffa, D. Campanella, L. Fratini, and F. Micari, Single block 3D numerical model for linear friction welding of titanium alloy, *Sci. Technol. Weld. Join.*, 24(2019), No. 2, p. 130.

[87] P.H. Geng, G.L. Qin, J. Zhou, and Z.D. Zou, Finite element models of friction behaviour in linear friction welding of a Ni-based superalloy, *Int. J. Mech. Sci.*, 152(2019), p. 420.

[88] K. Yonekura, T. Shinohara, and K. Masaki, Cost-effective estimation of flash extrusion and defects in linear friction welding using Voronoi diagrams, *J. Manuf. Process.*, 68(2021), p. 158.

[89] X.W. Yang, W.Y. Li, Y.X. Xu, X.R. Dong, K.W. Hu, and Y.F. Zou, Performance of two different constitutive models and microstructural evolution of GH4169 superalloy, *Math. Biosci. Eng.*, 16(2019), No. 2, p. 1034.

[90] A. Vairis and N. Christakis, The development of a continuum framework for friction welding processes with the aid of micro-mechanical parameterisations, *Int. J. Model. Identif. Contr.*, 2(2007), No. 4, art. No. 347.

[91] P.H. Geng, G.L. Qin, and J. Zhou, A computational modeling of fully friction contact-interaction in linear friction welding of Ni-based superalloys, *Mater. Des.*, 185(2020), art. No. 108244.

[92] P.H. Geng, G.L. Qin, C.G. Li, H. Wang, and J. Zhou, Study on the importance of thermo-elastic effects in FE simulations of linear friction welding, *J. Manuf. Process.*, 56(2020), p. 602.

[93] P.H. Geng, H. Ma, M.X. Wang, *et al*., Dissimilar linear friction welding of Ni-based superalloys, *Int. J. Mach. Tools Manuf.*, 191(2023), art. No. 104062.

[94] M. Javidikia, M. Sadeghifar, H. Champliaud, and M. Jahazi, Grain size and temperature evolutions during linear friction welding of Ni-base superalloy Waspaloy: Simulations and experimental validations, *J. Adv. Join. Process.*, 8(2023), art. No. 100150.

[95] F. Masoumi, D. Shahriari, H. Monajati, *et al*., Linear friction welding of AD730™ Ni-base superalloy: Process-microstructure-property interactions, *Mater. Des.*, 183(2019), art. No. 108117.

[96] S. Tabaie, F. Rézaï-Aria, B.C.D. Flipo, and M. Jahazi, Grain size and misorientation evolution in linear friction welding of additively manufactured IN718 to forged superalloy AD730™, *Mater. Charact.*, 171(2021), art. No. 110766.

[97] S. Tabaie, Farhad R. Aria, B.C.D. Flipo, and M. Jahazi. Dissimilar linear friction welding of selective laser melted Inconel 718 to forged Ni-based superalloy AD730TM: Evolution of strengthening phases. *J. Matei. Sci. Technol.*, 96(2022), p. 248.

[98] P.H. Geng, G.L. Qin, T.Y. Li, J. Zhou, Z.D. Zou, and F. Yang, Microstructural characterization and mechanical property of GH4169 superalloy joints obtained by linear friction welding, *J. Manuf. Process.*, 45(2019), p. 100.

[99] P.H. Geng, G.L. Qin, H. Ma, J. Zhou, and N.S. Ma, Linear friction welding of dissimilar Ni-based superalloys: Microstructure evolution and thermo-mechanical interaction, *J. Mater. Res. Technol.*, 11(2021), p. 633.

[100] A. Chamanfar, M. Jahazi, J. Gholipour, P. Wanjara, and S. Yue, Analysis of integrity and microstructure of linear friction welded Waspaloy, *Mater. Charact.*, 104(2015), p. 149.

[101] M. Smith, J.B. Levesque, L. Bichler, D. Sediako, J. Gholipour, and P. Wanjara, Residual stress analysis in linear friction welded in-service Inconel 718 superalloy via neutron diffraction and contour method approaches, *Mater. Sci. Eng. A*, 691(2017), p. 168.

[102] F. Masoumi, L. Thébaud, D. Shahriari, *et al*., High temperature creep properties of a linear friction welded newly developed wrought Ni-based superalloy, *Mater. Sci. Eng. A*, 710(2018), p. 214.

[103] X.W. Yang, C. Peng, T.J. Ma, *et al*., Finite element analysis of fatigue crack growth of linear friction welded superalloy joints, *Acta Aeronaut. Astronaut. Sin.*, 43(2022), No. 2, art. No. 625004.

[104] J.W. Chen, E. Salvati, F. Uzun, *et al*., An experimental and numerical analysis of residual stresses in a TIG weldment of a single crystal nickel-base superalloy, *J. Manuf. Process.*, 53(2020), p. 190.

[105] H. Pasiowiec, B. Dubiel, R. Dziurka, *et al*., Effect of creep deformation on the microstructure evolution of Inconel 625 nickel-based superalloy additively manufactured by laser powder bed fusion, *Mater. Sci. Eng. A*, 887(2023), art. No. 145742.

[106] S.M. Wen, Z.C. Liu, D. Mi, S.H. Yang, B.C. Li, and C. Jiang, Novel fatigue life prediction method of a Ni-based superalloy welded joint considering defect and temperature, *Int. J. Fatigue*, 177(2023), art. No. 107924.